JOURNAL OF GEOPHYSICAL RESEARCH, VOL. 114, C12027, doi:10.1029/2009JC005384, 2009

Click Here for Full Article

Phytoplankton blooms near the Pearl River Estuary induced by Typhoon Nuri

Hui Zhao,[1,2] DanLing Tang,[1,2] and Dongxiao Wang[1,2]

Received 14 March 2009; revised 21 August 2009; accepted 3 September 2009; published 30 December 2009.

[1] The authors investigate two phytoplankton blooms near or off the Pearl River Estuary (PRE) triggered by Category 2 Typhoon Nuri with moderate wind intensity in the South China Sea using both remotely sensed and in situ data sets. An offshore triangular phytoplankton bloom (chlorophyll *a* (Chl *a*) > 0.5 mg m^{-3}) was observed near Dongsha Archipelago along Nuri's track, prolongating southeastward to 18°N 1 week after the typhoon's passage; a stronger nearshore phytoplankton increase (Chl *a* > 1.5 mg m^{-3}) with high total suspended sediment appeared southwest of the PRE from the coast toward the South China Sea. After the typhoon's passage, sea surface cooling (~3°C), strong wind (>20 m s^{-1}), and heavy rainfall (>100 mm d^{-1}) were also observed in the region, especially offshore. In addition, the freshwater discharge from the PRE during the typhoon passage increased fivefold in comparison with the August climatology in the nearshore bloom region. The nearshore bloom was probably due to the increased discharge from the PRE and favorable current, as well as mixing, upwelling, and near-inertial resonance driven by strong typhoon wind. The offshore bloom may be triggered by upwelling and entrainment induced by strong typhoon wind and the topography of islands and islets. The present study suggests that one typhoon may nourish phytoplankton biomass by inducing transport of nutrient-rich water from both the Pearl River Estuary to offshore and the sublayer to surface.

Citation: Zhao, H., D. L. Tang, and D. Wang (2009), Phytoplankton blooms near the Pearl River Estuary induced by Typhoon Nuri, *J. Geophys. Res.*, *114*, C12027, doi:10.1029/2009JC005384.

1. Introduction

[2] A typhoon is an extremely strong wind event, which can have dramatic effects on the upper ocean. Typhoon-induced winds can cause entrainment, strong vertical mixing, and upwelling, as well as the cooling of near-surface water on the right-hand side of the storm track [*Hazelworth*, 1968; *Dickey and Simpson*, 1983; *Stramma et al.*, 1986; *Sanford et al.*, 1987; *Price*, 1981; *Emanuel*, 1999]. Typhoons also play an important role in phytoplankton blooms and primary productivity in typhoon-dominated oligotrophic oceanic waters [e.g., *Lin et al.*, 2003; *Babin et al.*, 2004; *Walker et al.*, 2005; *Zheng and Tang*, 2007; *Wang and Zhao*, 2008]. Typhoons or tropical cyclones occur frequently in the South China Sea (SCS), over seven annually on average; they can trigger sea surface cooling and phytoplankton blooms near their paths in the SCS, through oceanic eddies, mixing, and upwelling, as well as topography [*Chang et al.*, 1996; *Chen et al.*, 2003; *Lin et al.*, 2003; *Zheng and Tang*, 2007; *Chang et al.*, 2008; *Zhao et al.*, 2008]. Cyclones and typhoons have important effects on chlorophyll *a* (Chl *a*) or phytoplankton blooms with a contribution of 20–30% of the annual new production in the SCS. *Zheng and Tang* [2007] showed that Typhoon Damrey during September 2005 triggered two phytoplankton blooms in northern SCS via upwelling, vertical mixing, and increased terrestrial runoff, which supplied nutrients to the surface layer from depth and from land. However, previous studies mostly focused on the effects of typhoons on phytoplankton (i.e., Chl *a*) or primary productivity in offshore regions of the SCS; the possible effects of typhoons on phytoplankton near the Pearl River Estuary (PRE) have not been well investigated.

[3] The Pearl River, the second largest river (in terms of freshwater discharge) in China, stretches over 2200 km. Its average discharge is 10,524 m^3 s^{-1}, with 80% of the discharge occurring during April–September [*Zhao*, 1990]. The PRE is situated north of the SCS (Figure 1a), mainly influenced by the following three regimes: the PRE discharge, seawater from the SCS, and coastal waters [*Williamson*, 1970; *Morton and Wu*, 1975; *Mao et al.*, 2004]. In comparison to seawater, river water contains higher concentration of nutrients and suspended sediments [*Yin et al.*, 2004] and, therefore, could be an important source of nutrient materials to northern SCS. The impact of the river water in summer is limited to coastal regions because coastal currents generally cannot transport rich nutrients farther into the open sea [*Watts*, 1971, 1973]. Because of the effects of fluvial flux on inorganic carbon

[1]LED, South China Sea Institute of Oceanology, Chinese Academy of Sciences, Guangzhou, China.
[2]College of Earth Science, Graduate University of the Chinese Academy of Sciences, Beijing, China.

Copyright 2009 by the American Geophysical Union.
0148-0227/09/2009JC005384$09.00

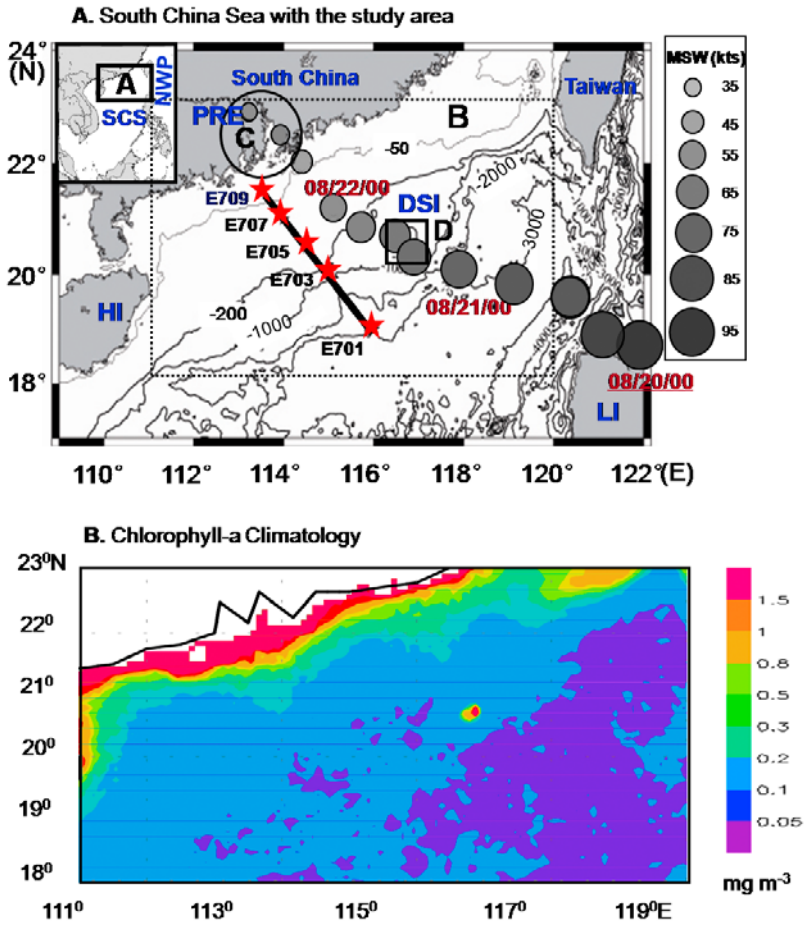

Figure 1. (a) Location of the study area and location and track of Typhoon Nuri in northern SCS. (b) Merged August Chl *a* climatology (mg m^{-3}) averaged over 2000–2007 dervied from SeaWiFS and Moderate Resolution Imaging Spectroradiometer-Aqua. In Figure 1a, box a is the location of northern SCS; DSI, Dongsha Island; PRE, Pearl River Estuary; HI, Hainan Island; LI, Luzon Island; kts, knots; MSW, maximum sustained wind (in knots;1 knot = 0.514 m s^{-1}); NWP, Northwest Pacific Ocean. Also in Figure 1a, box b is the study area (111–120°E, 18–23°N), circle c (the solid circle) is PRE and box d is the location of Dongsha Island.

and nutrients [*Cai et al.*, 2004], high Chl *a* and primary productivity [*Revelante and Gilmartin*, 1976; *Fisher et al.*, 1988; *Cloern*, 1996; *Yin et al.*, 2004; *Zhao and Tang*, 2007; *Shen et al.*, 2008] were detected in nearshore regions. The impact of increased freshwater discharge during typhoon passage on phytoplankton of the northern SCS, however, has not been well documented.

[4] In the summer season, the northern SCS is generally stratified, tropical, and oligotrophic. Low phytoplankton biomass were suggested in this area by Sea-viewing Wide Field-of-view Sensor (SeaWiFS)-derived Chl *a* concentration averaged for August 2000–2007 (Figure 1b). The increased Pearl River discharge, strong winds, and wind curls induced by a typhoon during its passage can exert important effects on the river-ocean interaction and the ecosystem of the northern SCS in summer. Nuri is a moderate Category 2 typhoon (which occurred in August 2008 in the SCS) that passed over the PRE. Quality Chl *a* data was available during this period because of the nearly cloud-free condition after the typhoon, which provides us with an opportunity to investigate the effect of a typhoon near the PRE on phytoplankton of the northern SCS with SeaWiFS-derived Chl *a* images and other satellite products, as well as in situ data. In this study, we first analyzed patterns of Chl *a*, sea surface temperature (SST), sea surface winds, total suspended sediment (TSS), and surface currents in the northern SCS during Typhoon Nuri. We will present the influence of the typhoon on the phytoplankton blooms in the northern SCS, with an emphasis on evaluating the increased injection of river water into the bloom region south of the PRE and the possible mechanism of the bloom from the nearshore region to the open sea.

2. Data and Methods

2.1. Satellite Data, Typhoon Data, and in Situ Data

2.1.1. Satellite Data

[5] Merged Aqua-derived Chl *a* product with 9 km resolution was obtained from the Distributed Active Archive Center of NASA (ftp://oceans.gsfc.nasa.gov/Merged/). Daily level 3 Chl *a* product was used in this

study, which is calculated using the ocean chlorophyll 4 algorithm [*O'Reilly et al.*, 1998].

[6] SeaWiFS-derived total TSS was produced and analyzed as a proxy for determining the influence from terrestrial materials. From the daily SeaWiFS files (available at http://oceancolor.gsfc.nasa.gov/cgi), the normalized water-leaving radiance (nLw) 443 and 555 products were extracted. This was followed by the derivation of the daily composites of the two bands. TSS calculation was then made by using the daily images of the two bands and applying

$$\mathrm{TSS} = 3.2602 \times (\mathrm{R}_{443}/\mathrm{R}_{555})^{-3.9322} \quad (1)$$

as in the work of *Pan et al.* [1999]. Furthermore, the daily TSS images were processed into mean images to discuss variations of TSS during pre-Nuri and post-Nuri periods.

[7] Surface current data (i.e., absolute geostrophic velocities) were obtained from the Colorado Center for Astrodynamics Research (CCAR) at the University of Colorado (http://las.aviso.oceanobs.com/). The data set was generated from model mean and altimeter measurements from the TOPEX/POSEIDON and ERS-2 satellites by CCAR [*Le Traon and Morrow*, 2000].

[8] Daily rainfall rate data were derived from the Tropical Rainfall Measuring Mission (TRMM) Microwave Imager (TMI). They have a resolution of 0.25° by 0.25°. Because of the cloud-penetrating capacity of TMI, the measurements can overcome the influence of cloudy conditions [*Wentz et al.*, 2000]. Therefore, TMI data can provide continuous rainfall observations with a good resolution before, during, and after a typhoon or hurricane, which is particularly useful during a hurricane.

[9] A new generation of global high-resolution (<10 km) SST products was provided by the Group for High-Resolution SST (GHRSST). Every day, GHRSST global processing systems combine several complementary satellites and in situ SST data streams together and deliver integrated SST products with supporting data in a common network Common Data Form format. Here daily level 4 (L4) remote sensing system (RSS) microwave (MW) IR optimally interpolated (OI) SSTs with spatial resolutions of 9 km were used in the present study.

[10] Daily data of absolute geostrophic velocities derived from merged altimeter products (Jason-1, Envisat, ERS-1/ERS-2, Geosat Follow-On, and TOPEX/POSEIDON) are available at http://www.aviso.oceanobs.com. The altimeter data were produced by the Segment Sol Multimission Altimetry and Orbitography/Data Unification and Altimeter Combination System and distributed by Archiving, Validation, and Interpretation of Satellite Oceanographic data with support from the Centre National d'Etudes Spatiales, France.

2.1.2. Typhoon Data

[11] The typhoon track data used in this study were available from the Unisys Weather Web site (http://weather.unisys.com/hurricane/w_pacific/), which is based on the best hurricane track data issued from the Joint Typhoon Warning Center (JTWC). The data include the maximum sustained surface wind speed and the location of the hurricane center every 6 hours. The translation speed of a hurricane was thus estimated based on the position of its center every 6 hours in our analysis. The maximum sustained surface wind speeds are shown for the period of Typhoon Nuri (Figure 1a). The surface wind data are based on the microwave scatterometer SeaWinds on the Quick Scatterometer (QuikSCAT) satellite [*Liu et al.*, 2000]. The daily QuikSCAT data, including ascending and descending passes (available at http://poet.jpl.nasa.gov), were used to study Typhoon Nuri.

2.1.3. In Situ Data

[12] In situ Chl *a*, temperature, and salinity data were measured at five stations along Transect E7 (marked by stars in Figure 1a) by the South China Sea Open Cruise, R/V *Shiyan 3*, carried out by the South China Sea Institute of Oceanology, Chinese Academy of Sciences, south of the PRE during 16–18 August 2007 and 2–6 September 2008. The Chl *a* samples of 0.5–2 L were collected from the surface (2 m) to a depth of 100 m. Vertical profiles of temperature and salinity were monitored with an integrated conductivity, temperature, and depth sensor at the five stations. In the present study, we used only Chl *a* data at 25 m due to the absence of surface data.

2.2. Methodology

2.2.1. Sea Surface Wind Vectors

[13] To present the spatial-temporal variation of wind before and during Nuri, daily sea surface wind vectors were processed by combining the two ascending and descending passes and then the combined daily products were imaged on 19 and 21 August 2008, respectively. Time series of wind speeds were obtained by averaging daily data over the box shown in Figure 2h.

2.2.2. SST and Rainfall

[14] The images of SST and rainfall rate were imaged during Nuri to display the change of SST and rainfall rate during the pre-Nuri (1–19 August 2008) and post-Nuri (20 days after typhoon Nuri's passage, i.e., 22 August to 9 September 2008)/Nuri (20–21 August) periods.

2.2.3. Chl *a* Concentration and TSS

[15] Chl *a* concentrations and TSS were first averaged over the following two periods: the pre-Nuri and post-Nuri period. The post-Nuri period was chosen because phytoplankton blooms generally appear several days after a storm, last 3–4 weeks, and decay to the prestorm level after about 1month and because there are generally relatively sparse observations of Chl *a* due to cloudy weather conditions [*Lin et al.*, 2003; *Zheng and Tang*, 2007; *Zhao et al.*, 2008].

2.2.4. In Situ Data

[16] In situ data of Chl *a*, temperature, and salinity (Table 1) observed during 2007 and 2008 were used for the offshore phytoplankton bloom region (E7 in Figure 1a). Vertical profiles of temperature and salinity were produced along Transect E7 for 2007 and 2008, respectively. The analysis of the in situ data can provide some useful information for probing into the bloom near the PRE. In addition, in order to evaluate the validity of satellite ocean color in the study, we chose some small square regions (about 81 km^2 per region), which were centered on the location of station E7, and extract satellite data from the Chl

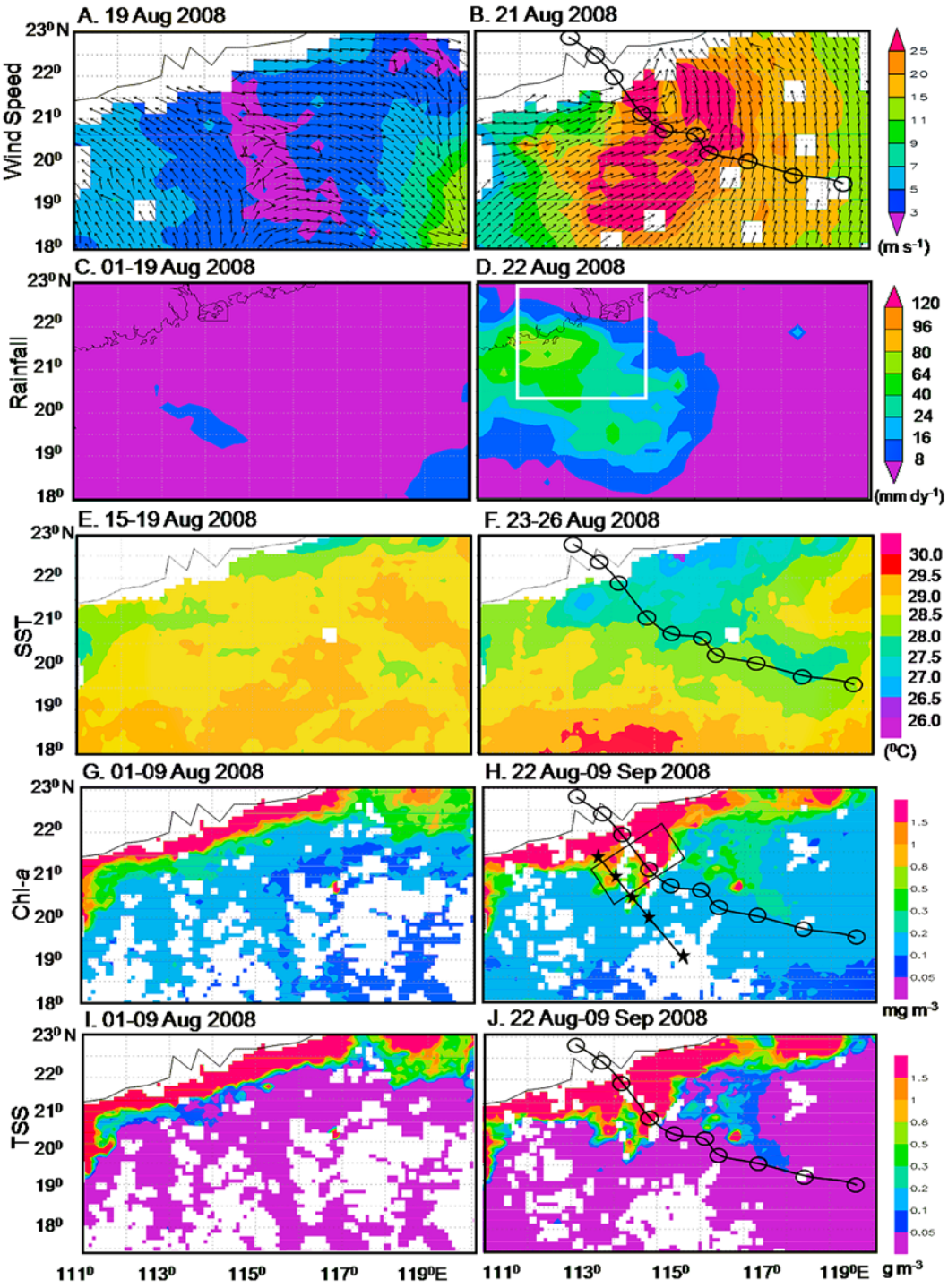

Figure 2. Images (a, c, e, g, and i) before Typhoon Nuri and (b, d, f, h, and j) during/after Typhoon Nuri. QuikSCAT surface wind vectors (m s^{-1}; Figures 2a and 2b), TRMM rainfall (mm d^{-1}; Figures 2c and 2d), GHRSST L4 RSS MW IR OI SST (°C; Figures 2e and 2f), merged Chl *a* concentrations (mg m^{-3}; Figures 2g and 2h), and SeaWiFS-derived TSSs (g m^{-3}; Figures 2i and 2j). The tracks indicate the passage of Typhoon Nuri in Figures 2b, 2f, 2h, and 2j.

a data averaged for 22 August to 9 September 2008 based on the responding regions.

2.2.5. Time Series of Satellite Data

[17] To investigate the relationship between Chl *a* concentration and oceanic conditions, we chose the box in Figure 2h for the time series of the during Nuri period, where the variations of Chl *a* and TSS were more notable. Time series of wind speed, SST, Chl *a*, and TSS averaged over the box during 10 August to 6 September 2008 were obtained, when the changes were more evident in the box.

Table 1. Information on In Situ Measurements at Different Stations During 2007 and 2008

Station	Station's Location	2008	2007
E701	116.00°E, 19.00°N	0305 Sep 2	0845 Aug 18
E703	115.00°E, 20.00°N	0541 Sep 3	1915 Aug 17
E705	114.50°E, 20.50°N	2041 Sep 5	0403 Aug 17
E707	114.00°E, 21.00°N	0248 Sep 6	2137 Aug 16
E709	113.50°E, 21.50°N	0850 Sep 6	1642 Aug 16

We also used TRMM rainfall data averaged in the region (20–23°N, 112–115°E) near the PRE for the time series to evaluate the variation of the PRE discharge.

3. Results

3.1. Wind Variation

[18] Nuri was a Category 2 typhoon (according to the Saffir-Simpson hurricane scale), which originated from the tropical depression in the Northwest Pacific (14.7°N, 140.8°E) on 1300 UTC on 17 August 2008, strengthened to a typhoon at 1200 UTC on 18 August with the strongest wind speed near the Luzon Island, and traversed the SCS from the coastlines north of the Luzon Island to the PRE from 0000 UTC on 20 August to 1200 UTC on 22 August 2008.

[19] The wind vector image (Figure 2a) on 19 August 2008 displayed that the wind was weak (<7 m s^{-1}) north of the SCS before Nuri's intrusion into the SCS and even weaker (<3 m s^{-1}) south of the PRE and (<5 m s^{-1}) northwest of the northern SCS. Here, we chose an image of the wind vector on 21 August (Figure 2b) to represent the wind during the typhoon. During Nuri's intrusion into the northern SCS, the strong wind (>11 m s^{-1}, Figure 2b) prevailed over the entire northern SCS, and the intensity of wind speed (Figures 1a and 2b) was strong (>25 m s^{-1}) along Nuri's track, which was followed by a weakening tendency from 48.82 m s^{-1} at 0000 UTC on 20 August to 23.13 m s^{-1} at 0600 UTC on 22 August. It traveled with a mean moving speed of 4.767 m s^{-1} (under a mean maximum wind speed of 32.5 m s^{-1}), a relatively slow moving speed of 3.55 m s^{-1} (under a mean maximum wind speed of 33.4 m s^{-1}) from 0600 to 1200 UTC on 21 August (i.e., near the Dongsha Islands), and a relatively fast moving speed of 4.37 m s^{-1} (under a mean maximum wind speed of 23.13 m s^{-1}) from 0000 to 1200 UTC on 22 August (i.e., near the PRE).

3.2. Rainfall and SST

[20] Before Nuri's passage, the mean rain is generally low (<16 mm d^{-1}) in northern SCS and even lower (<8 mm d^{-1}) in other regions (Figure 2c). During Nuri, the rainfall (>40 mm d^{-1}) around the area to the left of the typhoon's passage increased to 5–10 times (Figure 2d) that of the pre-Nuri rainfall (Figure 2c). At 0600 UTC on 22 August, the most intensive storm rain (~10 m h^{-1}) was located near the PRE, roughly centered at (112°E, 21.5°N; Figure 2d).

[21] The SST averaged for 15–18 August suggested that high temperature (>28.5°C) prevailed in the northern SCS under the condition of no typhoon (Figure 2e). The falling tendency of SST was evident after the typhoon in the northernmost SCS (Figure 2f). After the typhoon, a low SST patch (<27.5°C) appeared to the right of Nuri's path (Figure 2f), roughly a decrease of 1–3°C, especially near the PRE and Dongsha Archipelago.

3.3. Chl *a* and TSS

[22] The Chl *a* climatology displayed that August Chl *a* concentrations presented a gradual falling tendency from nearshore regions to offshore regions in the northern SCS (Figure 1b). There were higher Chl *a* (>1.5 mg m^{-3}) in a rough range of 50 km from the coastlines and lower Chl *a* (<0.2 mg m^{-3}) in offshore regions. The Chl *a* image averaged from 1–19 August (Figure 2g) displayed similar patterns to the August climatology, implying a low Chl *a* level (<0.2 mg m^{-3}) in offshore regions in August in general. After Nuri's passage, Chl *a* concentration averaged for 22 August to 9 September (Figure 2h) was obvious higher in the northernmost SCS, especially in offshore regions near the PRE (>1.2 mg m^{-3}) and Dongsha Archipelago (>0.3 mg m^{-3}), roughly coinciding with the patches of stronger wind speed, lower SST, and strong rainfall. In

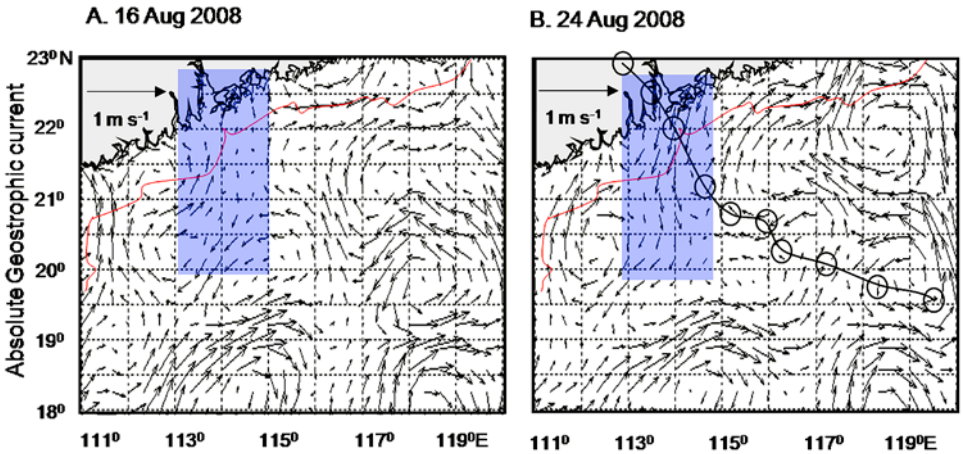

Figure 3. Absolute geostrophic current (m s^{-1}) (a) before and (b) after Typhoon Nuri. The tracks indicate the passage of Typhoon Nuri. Blue shading indicates the region with different current features before and after the typhoon; the red curve is the isobath of 50 m.

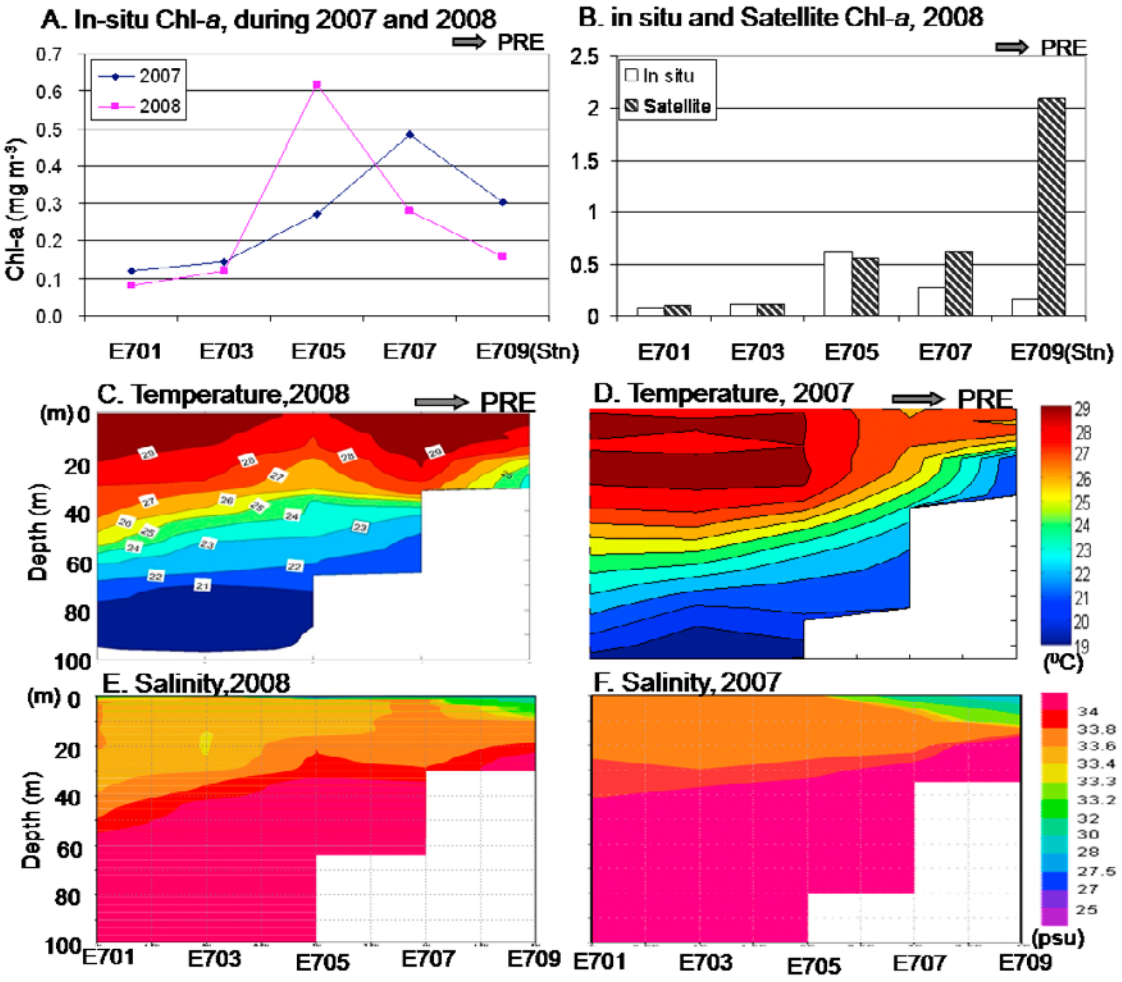

Figure 4. Comparisons of Chl *a*, temperature (°C), and salinity (practical salinity unit (psu)) along Transect E7 (stations marked by stars in Figure 1a) during 2008 and 2007. (a) Chl *a* comparison at 25 m depth (mg m^{-3}), (b) Chl *a* derived from in situ and satellite observations in 2008, (c and d) vertical temperature distribution (°C), and (e and f) vertical salinity distribution (psu). Merged satellite Chl *a* (Figure 4b).

the two bloom regions, a higher Chl *a* patch (more than 6 times that of the pretyphoon Chl *a*) near the PRE is more evident than (more than 2 times that of the pretyphoon Chl *a*) in the offshore region near the Dongsha Archipelago. Similar to Chl *a* distribution before and after the typhoon (Figures 2g and 2h), TSS displayed obvious increase (>0.1 g m^{-3}) in the two bloom regions near the PRE and Dongsha Archipelago after the typhoon's passage (Figures 2i and 2j), indicating generally elevated level of TSS.

3.4. Absolute Geostrophic Velocities

[23] There was an anticyclonic current in the northwestern SCS and two anticyclonic eddies south of 18 °N in August before Nuri's intrusion (Figure 3a). A weak southward current (<0.2 m s^{-1}) was observed from the PRE to 20°N. After the typhoon's passage, a strong southward current (>0.4 m s^{-1}) occurred south of the PRE all the way to 20°N (Figure 3b) with a location similar to that before the typhoon. The enhanced current can transport more rich nutrients from the estuary and coastal regions to offshore regions. Two eddies (Figure 3b) appeared near the Dongsha Archipelago, a cyclonic one around the archipelago and an anticyclonic one northeast of the archipelago. Between the two eddies, a northwestward current was evident to the left of the typhoon's track.

3.5. In Situ Data Along Transect E7

[24] The Chl *a* time series at 25 m depth displayed a high value (>0.6 mg m^{-3}) at Station 5 (E705 in Figure 1a) in 2008 coinciding with the bloom south of the PRE (Figure 4a), which did not appear in August 2007. In contrast, the Chl *a* values at the two stations near the PRE in 2007 were a little higher (>0.3 mg m^{-3}) than those in 2008 (0.1–0.3 mg m^{-3}). Comparison (Figure 4b) between satellite and in situ Chl *a* data in 2008 indicated that good correlations existed in the offshore regions (i.e., E701–E705), except for the coastal locations (i.e., E707 and E709). Stable stratification observed by the vertical profiles of temperature and salinity also suggested an oligotrophic status in the upper layer of the northern SCS (Figures 4c–4f). The swelling zones in Figures 4c and 4d near E705 indicated the existence of upwelling tendency at the station in summer 2008, which did not appeared in 2007 (Figures 4e and 4f). According to the patterns of temperature and

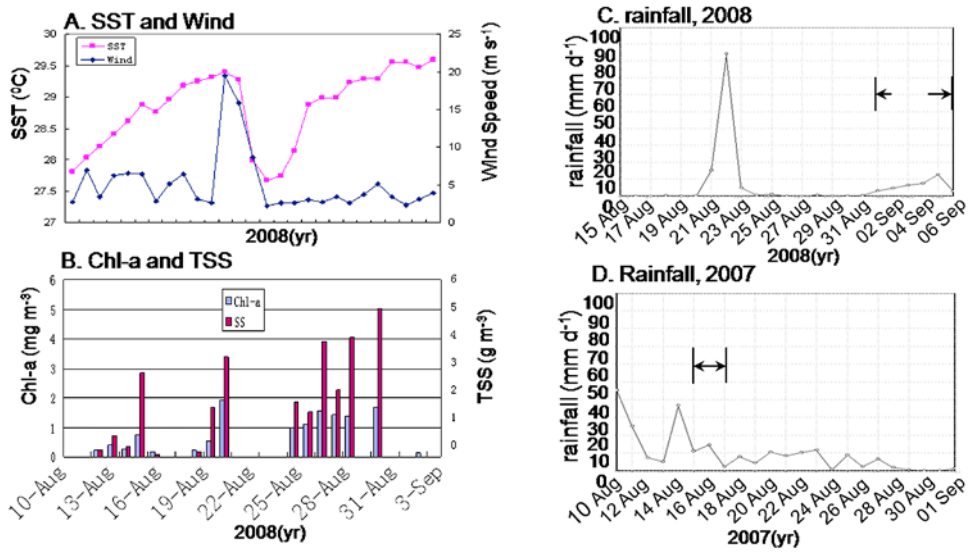

Figure 5. Time series of (a) Chl *a* (mg m^{-3}) and (b) TSS (g m^{-3}) based on a box offshore of the PRE in Figure 2h,and time series of rainfall for (c) 2008 (during Typhoon Nuri in mm d^{-1}) and (d) 2007 (corresponding period) based on the area average (20–23 °N, 112–115°E) in Figure 2d. The parts pointed by arrows in Figures 5c and 5d are the periods of the cruises.

salinity (Figures 4c–4f), for the upper 30 m layer, intrusion input of fresh water in 2008 was more evident than that in offshore regions (i.e., E701–E705); it was, however, weaker in coast regions (i.e., E707–709) compared with 2007.

3.6. Time Series of SST, Wind, Chl *a*, TSS, and Rainfall

[25] Decrease of SST is significant, with a maximum reduction of 2.5°C 3 days after the typhoon's passage on 25 August (Figure 5a). The speed (<8 m s^{-1}) was weak during the pretyphoon and posttyphoon period (Figure 5a). The wind speed was strong (>18 m s^{-1}) during the typhoon, up to 20 m s^{-1} on 22 August.

[26] Before the typhoon's passage, there were generally low concentrations of TSS (mean values < 1.2 g m^{-3}) and Chl *a* (mean values < 0.37 mg m^{-3}). Increasing concentrations of Chl *a* (mean values of 1.2 mg m^{-3}) and TSS (mean values of 3.1 g m^{-3}) after Nuri was generally observed in the region (Figure 5b). The results may indicate that a greater volume of nutrient-rich water from terrestrial runoff with high concentration of TSS were transported to the region.

[27] There was seldom rainfall (<5 mm d^{-1}) during most of August 2008 (Figure 5c); however, intensive storm rainfall (~85 mm d^{-1}) occurred near the PRE during the typhoon's passage. The rainfall of August 2007 (Figure 5d) was, however, generally higher than that of 2008, except during the typhoon period. According to the rainfall time series of 2008 and 2007, the rainfall was evidently stronger (mean rainfall of 20 mm d^{-1}) in the 7 days before the 2007 cruise than that (<11 mm d^{-1}) of the 2008 cruise.

4. Discussion

4.1. Typhoon-Induced Phytoplankton Blooms in Two Regions

[28] The Chl *a* concentration evidently increased after the typhoon's passage in the northern SCS, especially in the two regions south of the PRE and east of the Dongsha Archipelago. The patches of high Chl *a* blooms were showing up for 15 days. Typhoons can trigger phytoplankton blooms or high primary production where the strongest wind speeds and slowest moving speed occur [*Lin et al.*, 2003; *Babin et al.*, 2004; *Walker et al.*, 2005; *Zheng and Tang*, 2007; *Zhao et al.*, 2008], due to uptake of nutrient-rich waters from the depth through entrainment, mixing, Ekman pumping, or inertial resonances. In the present study, two phytoplankton blooms appeared, however, south of the estuary and near the archipelago (roughly around the typhoon track), instead of where the strongest wind speeds and slowest moving speeds occurred. This implies some other important factors induced the two blooms.

[29] According to previous studies [e.g., *Zhao et al.*, 2008], the phytoplankton blooms in offshore deep oceans appeared in these regions with stronger wind speed and slower moving speed during the typhoon's passage. In the bloom regions near the PRE, typhoon wind speed was weaker and moving speed was relative faster. The rainfall during the typhoon (Figure 2d) was over 5 times that of before the typhoon (Figure 2c) near the estuary, implying rapid increase in the discharge from the river. Rainfall averaged for the PRE (20–23°N, 112–115°E) also displayed significant increase during the typhoon (Figure 5c), suggesting the typhoon induced dramatic increase of the PRE discharge. The increased discharge can support the bloom south of the estuary. Moreover, the current south of the PRE was weak and northward before the typhoon, while after the typhoon a strong southward current from the estuary was observed (Figure 3b). This southward current can transport the coastal water or the discharge from the estuary into the northern SCS. In comparison to seawater, river water contains concentrations of nutrients orders of magnitude higher [*Yin et al.*, 2004] and suspended sediments [*Milliman and Meade*, 1983]. The higher TSS (Figure 2j) in the bloom region after the typhoon also suggested that the discharged water or coastal water with

high suspended sediment may intrude southward up to 20°N south of the PRE. Thus, the significant increase in discharge after the typhoon and the strong southward current played an important role in triggering the bloom near the estuary.

[30] In the other bloom region east of the Dongsha Archipelago, an appropriate water depth, a steep slope (Figure 1a), and a strong cyclonic boundary current were observed (Figure 3b). These conditions favor upwelling of deep water under the influence of typhoon wind speed and topography. On the side, there was relatively stronger wind speed (33.4 m s^{-1}) and slower moving speed (3.55 m $^{-1}$) of he typhoon. Thus, under the influence of island effects and strong wind, the conditions of stronger wind speed and slower moving speed [*Zhao et al.*, 2008] induced more prevailing upwelling and stronger mixing or near-inertial resonance during/after the typhoon's passage, as well as input of scouring water of ocean wave and rainfall for the archipelago, leading to the phytoplankton bloom in the region. In addition, there were a cyclonic eddy to the left of the bloom and an anticyclonic eddy to the right of the bloom, between which a northwestward current was induced/reinforced, leading to the northwestward transport of high phytoplankton biomass. The change of TSS indicated limitation of influence of river runoff near the Dongsha Archipelago in the offshore bloom region. Compared with the bloom region south of the PRE, the offshore phytoplankton bloom may be induced by local upwelling/mixing and near-inertial resonance, as well as its topography, instead of discharge from the river estuary.

4.2. Nearshore Phytoplankton Bloom Induced by the PRE Discharge

[31] The Chl *a* displayed high concentration at 25 m depth (Figure 4a) in Station 5 (E705 in Figure 1a) coinciding with the bloom offshore of the PRE in 2008 (Figure 2h). The good consistent tendency between the cruise data and the satellite data in most of the stations suggested it is roughly feasible using satellite Chl *a* in the present study and also confirmed the existence of the phytoplankton bloom near the PRE. Generally, there is higher salinity below the surface in the northern SCS [*Boyer et al.*, 2006] and lower salinity in regions affected by river waters. Thus, obvious gradient changes in the vertical profiles of temperature and salinity (Figures 5b and 5c) also indicated large freshwater input (Figures 4c–4e) for the upper 30 m layer in the region and the existence of upwelling tendency suggested by the doming zones of isotherms (Figure 4e) and isohalines (Figure 4d) near E705. It indicated that the nutrient-rich water reached the region and there was prevailing upwelling tendency at E705 in summer 2008. The relatively low concentrations in stations E707 and E709 (Figure 1a) close to the PRE, may be associated with high TSS and light limitation because productivity due to high dilution and light limitation was caused by high turbidity in the freshwater-dominated estuary [*Yin et al.*, 2004; *Milliman and Meade*, 1983], which can obviously lead to high estimations of satellite ocean color products, as observed in Figure 4b. There were obvious high SST (mean SST > 28.7°C) and weak wind speed (<6 m s^{-1}) before the typhoon. Because of stronger surface wind speed (17 $\sim$ 20 m s^{-1}) and related decreasing temperature (27.5 $\sim$ 28°C), the mixing/upwelling tendency [*Lin et al.*, 2003; *Zheng and Tang*, 2007; *Zhao et al.*, 2008] may be prevailing during Typhoon Nuri. High TSS after Nuri (Figure 5b) also indicated that discharge from the PRE can influence the region. However, compared with the pretyphoon TSS (Figure 5b), it suggests that nutrient-rich water from the terrestrial runoff can support the bloom in the region. Moreover, the higher salinity (Figure 4f) and rainfall (Figure 5d) during the cruise of 2007 also indicated more input from the PRE discharge in 2008 after the typhoon. The phenomena implied that increasing discharge from the estuary associated with favorable current direction exerted an important effect on the phytoplankton bloom, as mentioned in the work of *Yuan et al.* [2004].

[32] In addition, abundance of phytoplankton in euphotic zones generally depends on various physical, chemical, and biological factors. Among the physical variables, turbulence (mixing) in the water column plays a major role in uptake of nutrient-rich water, especially for shallow continental regions. For the shallow bloom region (<100 m, Figure 2h), strong wind stress also evidently influenced Chl *a* concentration and production, because of its contribution to the dynamics of the upper layer (i.e., waves, currents, shear, turbulence, etc.) [*Takahashi et al.*, 1977; *Pingree et al.*, 1978; *Therriault et al.*, 1978; *Klein and Coste*, 1984]. Thus, strong wind stress of the typhoon and increased discharge from the PRE, as well as a favorable cross-shelf current also played an important role in increased Chl *a* concentration south of the PRE.

5. Conclusion

[33] Two phytoplankton blooms were observed after Typhoon Nuri, one nearshore south of the PRE and one offshore east of the Dongsha Archipelago. The nearshore bloom was mainly due to the increased discharge from the PRE and a strong southward current from the Pearl River after the typhoon's passage, as well as mixing and upwelling driven by strong typhoon wind. The offshore bloom may have been triggered by upwelling and entrainment induced by strong typhoon wind and the topography of islands. By these mechanisms, one typhoon may induce transport of nutrient-rich water from depth and from the coast to offshore regions, nourishing phytoplankton biomass.

[34] **Acknowledgments.** This study was supported by the following programs and projects: (1) Chinese Academy of Sciences (CAS) (kzcx2-yw-226), (2) Natural Science Foundation Guangdong, China (Team Research Project 8351030101000002), and Natural Science Foundation of China (U0733002), and (3) the CAS/SAFEA International Partnership Program for Creative Research Teams.

References

Babin, S. M., J. A. Carton, T. D. Dickey, and J. D. Wiggert (2004), Satellite evidence of hurricane-induced phytoplankton blooms in an oceanic desert, *J. Geophys. Res.*, *109*, C03043, doi:10.1029/2003JC001938.

Boyer, T. P., et al. (2006), *World Ocean Database 2005* [DVDs], *NOAA Atlas NESDIS*, vol. 60, edited by S. Levitus, 190 pp., U.S. Gov. Print. Off., Washington, D. C.

Cai, W.-J., M. Dai, Y. Wang, W. Zhai, T. Huang, S. Chen, F. Zhang, Z. Chen, and Z. Wang (2004), The biogeochemistry of inorganic carbon and nutrients in the Pearl River Estuary and the adjacent northern South China Sea, *Cont. Shelf Res.*, *24*, 1301–1319, doi:10.1016/j.csr.2004.04.005.

Chang, J., C. C. Chung, and G.-C. Gong (1996), Influences of cyclones on chlorophyll *a* concentration and *Synechococcus* abundance in a subtropical

western Pacific coastal ecosystem, *Mar. Ecol. Prog. Ser.*, *140*, 199–205, doi:10.3354/meps140199.

Chang, Y., H.-T. Liao, M.-A. Lee, J.-W. Chan, W.-J. Shieh, K.-T. Lee, G.-H. Wang, and Y.-C. Lan (2008), Multisatellite observation on upwelling after the passage of Typhoon Hai-Tang in the southern East China Sea, *Geophys. Res. Lett.*, *35*, L03612, doi:10.1029/2007GL032858.

Chen, C. T. A., C. T. Liu, W. S. Chuang, Y. J. Yang, F. K. Shiah, T. Y. Tang, and S. W. Chung (2003), Enhanced buoyancy and hence upwelling of subsurface Kuroshio waters after a typhoon in the southern East China Sea, *J. Mar. Syst.*, *42*, 65–79, doi:10.1016/S0924-7963(03)00065-4.

Cloern, J. E. (1996), Phytoplankton bloom dynamics in coastal ecosystems: A review with some general lessons from sustained investigation of San Francisco Bay, California, *Rev. Geophys.*, *34*, 127–168, doi:10.1029/96RG00986.

Dickey, T. D., and J. J. Simpson (1983), The sensitivity of upper ocean structure to time varying wind direction, *Geophys. Res. Lett.*, *10*, 133–136, doi:10.1029/GL010i002p00133.

Emanuel, K. (1999), Thermodynamic control of hurricane intensity, *Nature*, *401*, 665–669, doi:10.1038/44326.

Fisher, T. R., L. W. Harding Jr., D. W. Stanley, and L. G. Ward (1988), Phytoplankton, nutrients and turbidity in the Chesapeake, Delaware and Hudson estuaries, *Estuarine Coastal Shelf Sci.*, *27*, 61–93, doi:10.1016/0272-7714(88)90032-7.

Hazelworth, J. B. (1968), Water temperature variations resulting from hurricanes, *J. Geophys. Res.*, *73*, 5105–5123, doi:10.1029/JB073i016p05105.

Klein, P., and B. Coste (1984), Effects of wind-stress variability on nutrient transport into the mixed layer, *Deep Sea Res., Part A*, *31*, 21–37, doi:10.1016/0198-0149(84)90070-0.

Le Traon, P. Y., and R. Morrow (2000), Ocean currents and eddies, in *Satellite Altimetry and Earth Sciences*, edited by L. L. Fu and A. Cazenave, pp. 171–215, Academic, San Diego, Calif.

Lin, I. I., W. T. Liu, C. Wu, G. T. F. Wong, C. Hu, Z. Chen, W. Liang, Y. Yang, and K. Liu (2003), New evidence for enhanced ocean primary production triggered by tropical cyclone, *Geophys. Res. Lett.*, *30*(13), 1718, doi:10.1029/2003GL017141.

Liu, T. W., X. Xie, P. S. Polito, S.-P. Xie, and H. Hashizume (2000), Atmospheric manifestation of tropical instability wave observed by QuikSCAT and tropical rain measuring mission, *Geophys. Res. Lett.*, *27*, 2545–2548, doi:10.1029/2000GL011545.

Mao, Q., P. Shi, K. Yin, J. Gan, and Y. Qi (2004), Tides and tidal currents in the Pearl River Estuary, *Cont. Shelf Res.*, *24*, 1797–1808, doi:10.1016/j.csr.2004.06.008.

Milliman, J. D., and R. H. Meade (1983), World-wide delivery of river sediment to ocean, *J. Geol.*, *91*, 1–21, doi:10.1086/628741.

Morton, B., and S. S. Wu (1975), The hydrology of the coastal waters of Hong Kong, *Environ. Res.*, *10*, 319–347, doi:10.1016/0013-9351(75)90029-8.

O'Reilly, J. E., S. Maritorena, B. G. Mitchell, D. A. Siegel, K. L. Carder, S. A. Garver, M. Kahru, and C. McClain (1998), Ocean color chlorophyll algorithms for SeaWiFS, *J. Geophys. Res.*, *103*, 24,937–24,953, doi:10.1029/98JC02160.

Pan, D., H. Haung, T. Mao, and Z. Mao (1999), Ocean color remote sensing by SeaWiFS in China, paper presented at 20th Asian Conference on Remote Sensing, Asian Assoc. of Remote Sens., Hong Kong, 22–25 Nov.

Pingree, R. D., P. M. Holligan, and G. M. Mardell (1978), The effects of vertical stability on the phytoplankton distributions in the summer on the northwest European shelf, *Deep Sea Res.*, *25*, 1011–1028, doi:10.1016/0146-6291(78)90584-2.

Price, J. F. (1981), Upper ocean response to a hurricane, *J. Phys. Oceanogr.*, *11*, 153–175, doi:10.1175/1520-0485(1981)011<0153:UORTAH>2.0.CO;2.

Revelante, N., and M. Gilmartin (1976), The effects of Po River discharge on phytoplankton dynamics in the northern Adriatic Sea, *Mar. Biol. Berlin*, *34*, 259–271, doi:10.1007/BF00388803.

Sanford, T. B., P. G. Black, J. R. Haustein, J. W. Feeney, G. Z. Forristall, and J. F. Price (1987), Ocean response to a hurricane. Part I: Observations, *J. Phys. Oceanogr.*, *17*, 2065–2083, doi:10.1175/1520-0485(1987)017<2065:ORTAHP>2.0.CO;2.

Shen, S., G. G. Leptoukh, J. G. Acker, Z. Yu, and S. J. Kempler (2008), Seasonal variations of chlorophyll a concentration in the northern South China Sea, *IEEE Geosci. Remote Sens. Lett.*, *5*(2), 315–319, doi:10.1109/LGRS.2008.915932.

Stramma, L., P. Cornillon, and J. F. Price (1986), Satellite observations of sea surface cooling by hurricanes, *J. Geophys. Res.*, *91*, 5031–5035, doi:10.1029/JC091iC04p05031.

Takahashi, M., D. L. Siebert, and W. H. Thomas (1977), Occasional blooms of phytoplankton during summer in Saanich Inlet, B. C., Canada, *Deep Sea Res.*, *24*, 775–780, doi:10.1016/0146-6291(77)90499-4.

Therriault, J.-C., D. J. Lawrence, and T. Platt (1978), Spatial variability of phytoplankton turnover in relation to physical processes in a coastal environment, *Limnol. Oceanogr.*, *23*, 900–911.

Walker, N. D., R. R. Leben, and S. Balasubramanian (2005), Hurricane-forced upwelling and chlorophyll *a* enhancement within cold-core cyclones in the Gulf of Mexico, *Geophys. Res. Lett.*, *32*, L18610, doi:10.1029/2005GL023716.

Wang, D. X., and H. Zhao (2008), Estimation of phytoplankton responses to Hurricane Gonu over the Arabian Sea based on ocean color data, *Sensors*, *8*, 4878–4893, doi:10.3390/s8084878.

Watts, J. C. D. (1971), A general review of the oceanography of the northern sector of the South China Sea, *Hong Kong Fish. Bull. 2*, pp. 41–50, Agric. and Fish. Dep., Hong Kong.

Watts, J. C. D. (1973), Further observation on the hydrology of the Hong Kong territorial waters, *Hong Kong Fish. Bull. 3*, pp. 9–35, Agric. and Fish. Dep., Hong Kong.

Wentz, F. J., C. Gentemann, D. Smith, and D. Chelton (2000), Satellite measurements of sea surface temperature through clouds, *Science*, *288*, 847–850, doi:10.1126/science.288.5467.847.

Williamson, G. R. (1970), The hydrography and weather of the Hong Kong fishing grounds, *Hong Kong Fish. Bull. 1*, pp. 43–49, Agric. and Fish. Dep., Hong Kong.

Yin, K., J. L. Zhang, P. Y. Qian, W. J. Jian, L. M. Huang, J. F. Chen, and M. C. S. Wu (2004), Effect of wind events on phytoplankton blooms in the Pearl River Estuary during summer, *Cont. Shelf Res.*, *24*, 1909–1923, doi:10.1016/j.csr.2004.06.015.

Yuan, J., R. L. Miller, R. T. Powell, and M. J. Dragg (2004), Storm-induced injection of the Mississippi River plume into the open Gulf of Mexico, *Geophys. Res. Lett.*, *31*, L09312, doi:10.1029/2003GL019335.

Zhao, H. (1990), *Evolution of the Pearl River Estuary* (in Chinese), 358 pp., China Ocean Press, Beijing.

Zhao, H., and D. L. Tang (2007), Effect of 1998 El Niño on the distribution of phytoplankton in the South China Sea, *J. Geophys. Res.*, *112*, C02017, doi:10.1029/2006JC003536.

Zhao, H., D. L. Tang, and Y. Wang (2008), Comparison of phytoplankton blooms triggered by two typhoons with different intensities and translation speeds in the South China Sea, *Mar. Ecol. Prog. Ser.*, *365*, 57–65, doi:10.3354/meps07488.

Zheng, G. M., and D. L. Tang (2007), Offshore and nearshore chlorophyll increases induced by typhoon and typhoon rain, *Mar. Ecol. Prog. Ser.*, *333*, 61–74, doi:10.3354/meps333061.

D. L. Tang, D. Wang, and H. Zhao, LED, South China Sea Institute of Oceanology, Chinese Academy of Sciences, 164 W. Xingang Rd., Haizhu District, Guangzhou 510301, China. (dxwang@scsio.ac.cn)